nature physics

SUPPLEMENTARY INFORMATION

https://doi.org/10.1038/s41567-019-0650-1

In the format provided by the authors and unedited.

Kibble–Zurek universality in a strongly interacting Fermi superfluid

Bumsuk Ko[1,2], Jee Woo Park[1*] and Y. Shin[1,2*]

[1]Department of Physics and Astronomy, Institute of Applied Physics, Seoul National University, Seoul, Korea. [2]Center for Correlated Electron Systems, Institute for Basic Science, Seoul, Korea. *e-mail: jw_park@snu.ac.kr; yishin@snu.ac.kr

Supplementary information for "Kibble-Zurek universality in a strongly interacting Fermi superfluid"

Bumsuk Ko,[1,2] Jee Woo Park,[1,*] and Y. Shin[1,2,†]

[1] *Department of Physics and Astronomy, and Institute of Applied Physics, Seoul National University, Seoul 08826, Korea*
[2] *Center for Correlated Electron Systems, Institute for Basic Science, Seoul 08826, Korea*

(Dated: July 23, 2019)

Temperature evolution in thermal quenching

The linear relationship between the sample temperature and the ODT beam intensity can be inferred by observing the evolution of the thermal cloud size in time-of-flight images from the experiment. Fig. S1 shows that the square of the thermal cloud size, which is proportional to the sample temperature, linearly decreases as the intensity is linearly reduced during the quench, and it remains constant after the quench is completed.

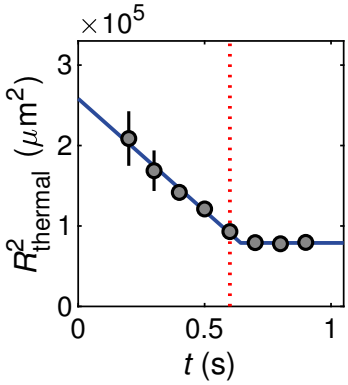

FIG. S1. **The evolution of the square of the thermal cloud size in the experiment.** Data obtained for $t_q = 600$ ms at $-1/k_F a = -1.53$. Each data point comprises ten realisations of the same experiment, and the error bars represent the standard deviation. The blue line is a bilinear fit to the data, where one of the lines is kept horizontal. The vertical dotted line marks the end of the quench.

Counting vortices in time-of-flight images

To extract the vortex number from TOF images, we use an automised image processing method, similar to the one outlined in Ref. [S1]. First, for a given absorption image, the contribution to the optical depth from the non-condensed fraction of the sample is removed by fitting a Gaussian to the thermal wings and subtracting it off. Then, a copy of this image is created, and a two-dimensional Gaussian smoothing filter is applied, whose width is chosen to be comparable to the typical size of a density depleted hole. This filtered image is used to divide the unfiltered image, which is then binarised using an empirically chosen threshold value that best identifies the density depleted holes as isolated "particles" (see Fig. S2). Using a standard particle analysis package included in most mathematical computing software (e.g. Matlab, Igor, Mathematica), the boundaries and the areas of the individual particles are identified. Fig. S3 exhibits exemplary TOF images taken from Fig. 1d of the main manuscript together with the processed images showing the boundaries of the density depleted holes, demonstrating the reliability of this procedure.

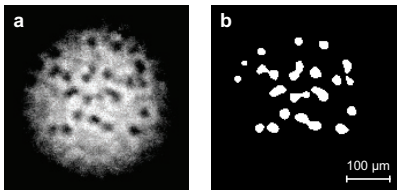

FIG. S2. **Creating a binary image of the density depleted holes. a** is an exemplary image of the optical depth of the sample after TOF, and **b** shows the converted binary image identifying the density depleted holes.

For samples that are densely populated by vortices, large holes that represent multiple vortices are observed. To assign a proper quanta, we plot the histogram of the hole area at each investigated interaction strength and assign a cut-off area for each quanta based on the multiple peak structure of the histogram (see Fig. S4). The minima between two adjacent peaks are used to set the vortex number transition lines of the particles. Based on this criteria, each particle is assigned a quanta equal to the number of vortices it represents, and their sum is recorded as the number of vortices of the image. Also, once the vortex number is determined by this procedure, every image was double-checked by eye to correct for possible misassignments.

Condensate formation and vortex decay

In the KZ mechanism, topological defects emerge in the system through the merging of domains with inde-

* jw_park@snu.ac.kr
† yishin@snu.ac.kr

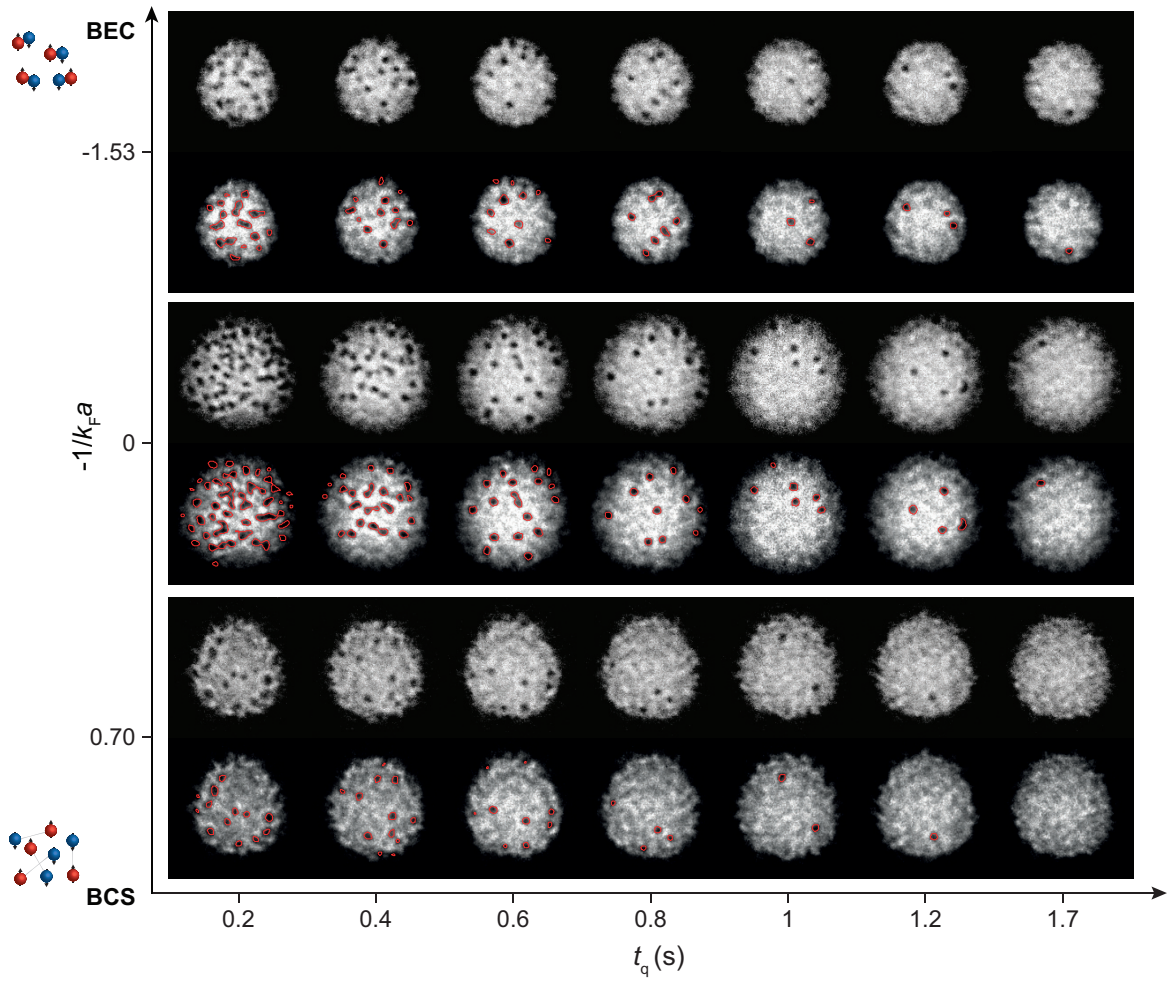

FIG. S3. **Computer-assisted counting of vortex number.** Images from Fig. 1d and when they are applied to the vortex counting procedure. Identified vortices are encircled by red lines.

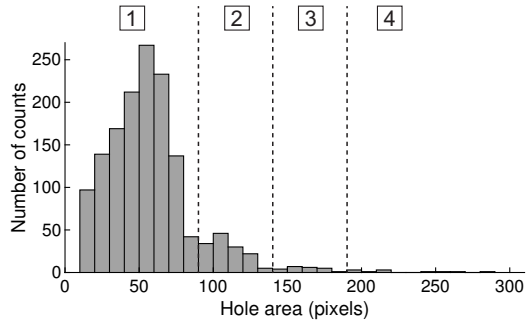

FIG. S4. **The histogram of the identified vortex areas.** The data consists of 70 images at unitarity, where the quench time extends between 200 ms to 800 ms.

pendent order parameters. To reliably extract the number of defects, a certain amount of hold time must be applied to the sample after the thermal quench to ensure that the condensate growth and the domain merging dynamics have been completed. However, in the presence of destructive interactions among the defects, this hold time must be kept as short as possible, such that the ensuing reduction of their numbers does not affect the observed scaling relationship between the defect density and the quench rate.

It should be noted that for the case of weakly interacting BECs, investigations on the effect of the dissipative evolution of the defects on the observed KZ scaling have shown that the KZ exponent is fairly robust against the decay of the defect number [S2, S3]. Nonetheless, to apply a well-defined hold time $t_{\rm h}$ to the sample before releasing it for TOF imaging, we investigate the evolution of the condensate fraction and the vortex number as a function of $t_{\rm h}$ for a number of quench times, at each the interaction strength accessed in the experiment.

The condensate fraction of the sample is measured using the "rapid-ramp technique," where prior to releasing the sample for TOF expansion, the Feshbach field is rapidly ramped to the molecular side of the resonance to convert the fermion pairs into tightly bound molecules.

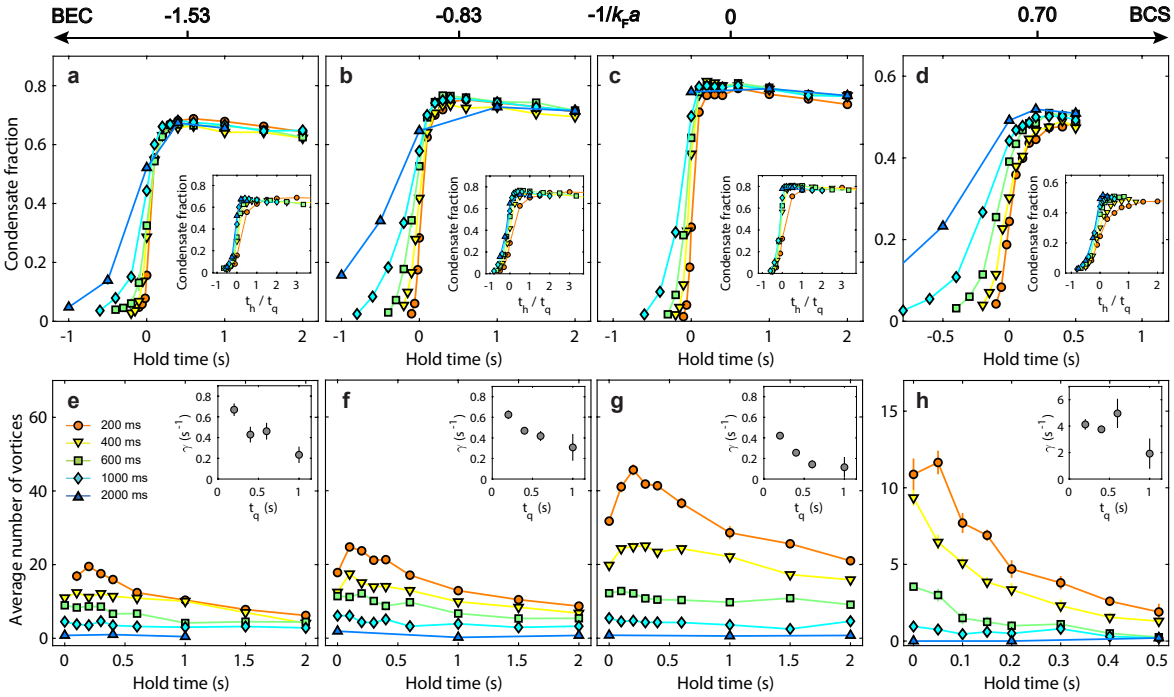

FIG. S5. **The evolution of the sample during and after various quench times t_q = 200 ms (circle), 400 ms (inverted triangle), 600 ms (square), 1000 ms (diamond), and 2000 ms (triangle). a-d**, The growth and decay of the condensate fraction of the sample during and after the quench. **e-h**, The decay of the average number of counted vortices during hold time t_h after the quench. Each data point is the average of ten realisations of the same experiment and the error bars give the standard error of the mean, where the unseen ones are hidden by the markers.

A bimodal fit is then applied to extract the condensate fraction, as shown in Fig. S5a-d. Generically, following the quench, the condensate fraction initially rises until it reaches a maximal value near $t_h = 200 \sim 300$ ms ($50 \sim 150$ ms for measurements on the BCS side), and then it decays due to three-body losses. This value of t_h may represent the intrinsic time scale for the condensate growth dynamics of the system. The condensate fraction measured after this hold time is independent of the quench time for each $-1/k_F a$, indicating that the sample is well thermalised during the quench for the investigated quench times. Also, when the hold time of each data set is normalised by its respective quench time (see insets of Fig. S5a-d), the evolution of the condensate fraction during the ODT ramp closely tracks each other for all the quench times apart from 200 ms, where it starts to show a weak deviation. This observation implies that the temperature of the sample is set by the ODT depth for the explored quench times during the quench.

The evolution of the vortex number shown in Fig. S5e-f displays a similar trend compared to that of the condensate fraction. Specifically, the area of the density depleted regions initially rises as the domains merge until it reaches a maximal value, and then it decays as the loss mechanism among the defects starts to dominate. Based on these observations, we set t_h to be the time at which the defect number reaches its maximum, corresponding to $t_h = 200$ ms for measurements performed on the BEC side of the resonance and at unitarity, and $t_h = 50$ ms for the data taken on the BCS side due to a faster decay rate.

An important observation is that the decay rate of the vortices is dependent on the initial vortex density set by the quench time t_q. Specifically, it becomes enhanced at short quench times where the initial vortex number is higher. The insets in Fig. S5e-h show the decay constant γ as a function of the quench time when we fit an exponential decay of the vortex number $N(t) = N_0 e^{-\gamma t}$ to the data whose hold time is equal to or greater than t_h. Here, t is the hold time and N_0 is the the hypothetical vortex number at $t = 0$. The increase in the exponential decay rate for shorter quench times reveals the presence of a beyond one-body decay mechanism, which likely arises from the destructive interactions among vortices with opposite charges. In the experiment, this loss mechanism is associated with the departure from the KZ scaling and the saturation of the vortex number for short quench times.

Dimensionality of the KZ domain formation

From the perspective of the KZ mechanism, the defect formation dynamics should be considered to be effectively 2D if the freeze-out correlation length $\hat{\xi}$ is longer than the

axial dimension of the sample. For our system at 757 G (corresponding to $a = 3981.8a_0$), taking the thermal de-Broglie wavelength $\lambda_{\mathrm{dB,c}} \approx 0.8$ μm at the critical point as the microscopic length scale ξ_0 for the correlation length and the (classical) elastic scattering time $1/n_0\sigma v \approx 36$ μs as the microscopic timescale τ_0 for the relaxation time, the freeze-out correlation length $\hat{\xi} = \xi_0(t_{\mathrm{q}}/\tau_0)^{\nu/(1+\nu z)}$ is estimated to be about 14 μm for the shortest quench time explored of 200 ms, compared to the axial size of the sample $R_z = \sqrt{\frac{2k_{\mathrm{B}}T_{\mathrm{c}}}{m_{\mathrm{mol}}\omega_z^2}} \approx 4$ μm. Here, n_0 is the central density of the molecules in the harmonic trap, $\sigma = 8\pi a_{\mathrm{mol}}^2$ is the scattering cross section of diatomic molecules, $a_{\mathrm{mol}} = 0.6a$ is the molecular scattering length, $v = \sqrt{3k_{\mathrm{B}}T_{\mathrm{c}}/m_{\mathrm{mol}}}$ is the root mean squared velocity of the molecules at T_{c}, $m_{\mathrm{mol}} = 2m$ is the molecule mass, and $\omega_z \approx 2\pi \times 1$ kHz is the axial trapping frequency. Hence, the domain formation dynamics will be initially 2D. However, as the condensation front moves away from the trap center during the quench and the local freeze-out correlation length decreases due to the decreasing local critical temperature, a dimensional crossover from 2D to 3D may occur. From a theoretical viewpoint, the KZ mechanism itself does not distinguish between the two scenarios, so the effect of this crossover should be weak, if it exists at all.

Mean-field critical velocity

The mean-field Landau critical velocity of a strongly interacting Fermi superfluid in the BEC-BCS crossover is given by $\min(v_{\mathrm{s}}, v_{\mathrm{pb}})$ where v_{s} is the speed of sound and v_{pb} is the mean-field BCS pair-breaking velocity of the superfluid [S4]. The speed of sound is obtained from the quantum Monte Carlo equation of state in Ref. [S5]. For our inhomogeneous superfluid sample in the harmonic potential, the critical velocity v_{c} at its centre is calculated by assuming the local density approximation. Here, the column averaged density, instead of the central density, has to be employed in computing v_{s} since the superfluid is hydrodynamic in the axial direction.

[S1] Kwon, W. J., Moon, G., Choi, J. Y., Seo, S. W. & Shin, Y. I. Relaxation of superfluid turbulence in highly oblate Bose-Einstein condensates. *Phys. Rev. A* **90,** 063627 (2014).

[S2] Donadello, S. *et al.* Creation and counting of defects in a temperature-quenched Bose-Einstein condensate. *Phys. Rev. A* **94,** 023628 (2016).

[S3] Liu, I. K. *et al.* Dynamical equilibration across a quenched phase transition in a trapped quantum gas. *Comm. Phys.* **1,** 24 (2018).

[S4] Combescot, R., Kagan, M. Y. & Stringari, S. Collective mode of homogeneous superfluid fermi gases in the BEC-BCS crossover. *Phys. Rev. A* **74,** 042717 (2006).

[S5] Manini, N. & Salasnich, L. Bulk and collective properties of a dilute Fermi gas in the BCS-BEC crossover. *Phys. Rev. A* **71,** 033625 (2005).